ELSEVIER

Nuclear Physics A 597 (1996) 327–340

NUCLEAR PHYSICS A

Ground-state properties of exotic Si, S, Ar and Ca isotopes

T.R. Werner[a,b,c], J.A. Sheikh[d,e], M. Misu[b], W. Nazarewicz[a,b,c], J. Rikovska[f,g], K. Heeger[f], A.S. Umar[h], M.R. Strayer[a,b]

[a] *Physics Division, Oak Ridge National Laboratory, P.O. Box 2008, Oak Ridge, TN 37831, USA*
[b] *Department of Physics and Astronomy, University of Tennessee, Knoxville, TN 37996, USA*
[c] *Institute of Theoretical Physics, Warsaw University, Hoża 69, 00-681 Warsaw, Poland*
[d] *Joint Institute for Heavy-Ion Research, P.O. Box 2008, Oak Ridge, TN 37831, USA*
[e] *Tata Institute of Fundamental Research, Colaba, Bombay 400 005, India*
[f] *Department of Physics, Oxford University, Parks Rd., Oxford OX1 3PU, UK*
[g] *Department of Chemistry, University of Maryland, College Park, MD 20742, USA*
[h] *Department of Physics, Vanderbilt University, Nashville, TN 37235, USA*

Received 28 September 1995; revised 21 November 1995

Abstract

Masses, deformations, radii, two-neutron separation energies and single-particle properties of Si, S, Ar and Ca isotopes are investigated in the framework of the self-consistent mean-field theory. In particular, the role of the $N = 28$ gap in the neutron-rich isotopes, and differences between proton and neutron deformations are discussed.

PACS: 21.10.-k, 21.60.Jz, 27.30.+t, 27.40.+z

1. Introduction

One of the most interesting challenges that confronts the nuclear physics community is the explanation of new phenomena that are expected in regions of extreme-isospin nuclei far from the valley of beta stability. This excursion into the yet unexplored part of the periodic chart will be possible thanks to new experimental techniques, and in particular radioactive nuclear beams [1–3].

Nuclei close to the particle drip lines exhibit a rich variety of properties which do not occur, or are much less pronounced, for nuclei close to the stability valley. The closeness of the unbound scattering states and extreme spatial extensions of weakly bound systems make neutron- or proton-rich nuclei very difficult to describe in terms of currently used

SSDI 0375-9474(95)00476-9

models with their parameters determined so as to reproduce the properties of stable nuclei [4–8].

In this paper, we discuss the ground-state properties of the Si, S, Ar and Ca isotopes, in particular those with a neutron number around the magic number 28, and the heaviest isotopes close to the neutron drip line. Some of the results (on the sulfur isotopes) have already been published [9]. The microscopic structure of these nuclei is of particular interest for astrophysics: the neutron-rich $N \approx 28$ nuclei play an important role in the nucleosynthesis of the heavy Ca–Ti–Cr isotopes [10]. As they also become experimentally accessible [10,11], they can provide a testing ground for studying exotic nuclei.

Of the nuclei considered here, those with $N = Z$ (^{28}Si, ^{32}S, ^{36}Ar and ^{40}Ca) have been studied extensively both theoretically and experimentally. Among different theoretical approaches used are the shell-correction approach [12], Hartree–Fock [13,14] and Hartree–Fock–Bogolyubov methods [15], relativistic mean field [16–19], shell model [20], α-cluster model [21] and others. Almost all these calculations give consistent ground-state deformations for the $N = Z$ nuclei: prolate for ^{32}S and oblate for ^{28}Si and ^{36}Ar.

Within the extreme spherical shell model, the Si, S, Ar and Ca isotopes are described in terms of the *sd* shell-model configurations for protons and *fp* configurations for neutrons. However, as discussed in Ref. [9], such a classification is far too simplified, since it neglects the core polarization effects associated with the core-breaking excitations [10,22]. Such excitations give rise to static shape deformations. In order to describe deformed configurations, one has to include into the analysis neutron excitation to the full *fp* shell [23–28]. For a review of nuclear deformations in this mass region, the reader is referred to Ref. [22] and references quoted in Ref. [9].

To shed some light on the physics of exotic neutron-rich nuclei with $N \approx 28$, we performed calculations based on the self-consistent mean-field theories: Hartree–Fock (HF) with the Skyrme effective interactions, and the relativistic mean-field (RMF) approach. The predicted separation energies and charge radii are compared to the available experimental data. Particular attention is paid to three topics: (i) the onset of deformation around the $N = 28$ magic gap, (ii) stability of the heaviest Si, S, Ar and Ca nuclei, and (iii) the isovector shape deformation effects.

2. Theoretical models

The first method employed in our analysis is the HF+Skyrme approach. We perform the HF calculations by discretizing the energy functional on a three-dimensional Cartesian spline collocation lattice [29,30] with no self-consistent symmetry imposed and the exchange Coulomb term in the Slater form. The correction for the center-of-mass motion is calculated by means of simple scaling of the nuclear mass. No projection on states of good angular momentum was performed. Both these corrections could introduce changes in calculated energies by a few hundred keV and shift the location of drip

lines by one or two units.

The calculations are performed in a cube of the size $(20\ \mathrm{fm})^3$. The SIII parametrization [31] of the Skyrme functional is used, but for comparison, some calculations have also been performed with the SkM* set of parameters [32].

In the relativistic mean-field (RMF) calculations, we use the model of Ref. [33] consisting of baryon (proton and neutron) and σ-, ω- and ρ-meson fields. The σ-meson is assumed to move in a non-linear potential

$$U(\sigma) = \tfrac{1}{2}m_\sigma\sigma^2 + \tfrac{1}{3}g_2\sigma^3 + \tfrac{1}{4}g_3\sigma^4. \tag{1}$$

In the present work, we have employed the NL-SH set of the Lagrangian density parameters [34], as this set has been claimed to be particularly successful in describing properties of very neutron-rich systems. The resulting Dirac equation for the baryons and the Klein–Gordon equations for the mesons were solved by expanding the small and large components of the Dirac spinor and the meson fields in the basis consisting of 12 harmonic oscillator shells. The expansion method in the harmonic oscillator basis does not allow for the correct description of the wave-function asymptotics in very neutron-rich nuclei but does not influence in practice the calculated energies and values of S_{2n}.

In both types of calculations (HF and RMF), the number of iterations was chosen individually for each nucleus, so as to ensure convergence within 5 keV in both total and single-particle energies.

In drip-line nuclei, the usual BCS approach gives rise to scattering of the nucleonic pairs from bound states to the continuum, thus leading to the presence of unphysical "particle gas" surrounding the nucleus [4]. In order to be able to describe such nuclei, one should use models in which the wave functions of occupied quasiparticle states have the correct asymptotic behavior. This can be achieved within the Hartree–Fock–Bogolyubov (HFB) method [4]. A precise, three-dimensional HFB code in space is not yet available. Therefore, in our calculations, the pairing Hamiltonian was approximated by a state-independent monopole pairing force. To minimize the effect of the neutron gas, the calculations were performed within constant-gap approximation. (The self-consistent treatment of the seniority-pairing interaction leads to an unphysical increase of pairing gaps in weakly bound nuclei due to increased density of positive energy quasibound states [6].) We have used two sets of pairing gaps, namely $\Delta_n = \Delta_p =$ 75 keV and 1 MeV in RMF calculations, and $\Delta_n = \Delta_p =$ 200 keV and 1 MeV in HF calculations. (As is well known, due to the occurrence of single-particle crossings, it is very difficult to get convergent results with no pairing at all.) By comparing results with weaker and stronger pairing, the effect of neutron gas and its influence on the global properties of the discussed nuclei could be investigated. The BCS equation for the Fermi level was solved using the lowest Z or N single-particle orbitals for protons or neutrons, respectively, counting from the bottom of the average potential well.

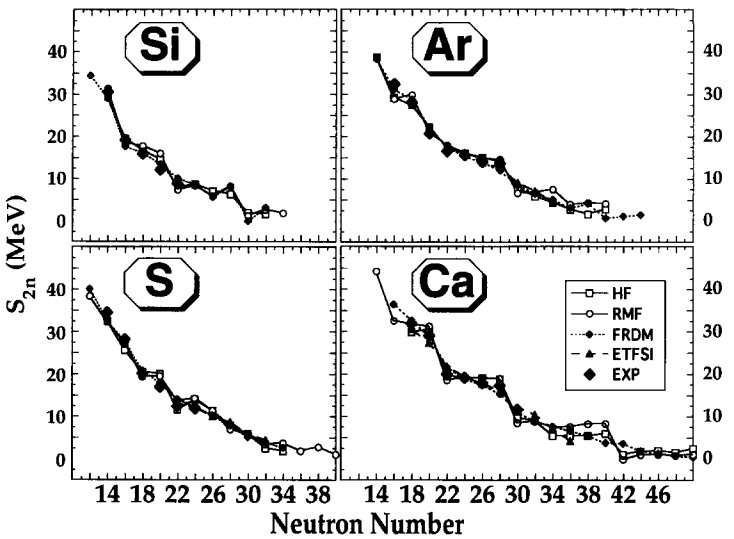

Fig. 1. Two-neutron separation energies of the even–even Si, S, Ar and Ca isotopes calculated with the RMF (open circles), HF (open squares), ETFSI (triangles) and FRDM (diamonds) models. Where available, the experimental values are indicated by large diamonds.

3. Results

3.1. Neutron drip line

For nuclei close to the neutron drip line, the neutron separation energy is of particular interest. The two-neutron separation energy is defined as

$$S_{2n}(N) = B(N,Z) - B(N-2,Z)$$

where $B(N,Z)$ is the binding energy of the nucleus (N,Z). For the nucleus to be stable against the two-neutron decay S_{2n} cannot be negative. The location of the two-neutron drip line for a given element is defined by the isotope with the largest value of N for which $S_{2n}(N)$ is still positive.

Figs. 1 and 2 display two-neutron separation energies for the Si, S, Ar and Ca isotopes. For comparison, curves corresponding to the finite-range droplet model (FRDM) [35] and the extended Thomas–Fermi with the Strutinsky-integral model (ETFSI) [36] are also shown. (For the elements considered in our study, ETFSI results for the most neutron-rich isotopes have not been available to us.) One can see that for nuclei for which experimental data are available, all models yield similar results. The detailed behavior of S_{2n} for the drip-line nuclei is illustrated in Fig. 2. To make the figure more readable, except for Ar isotopes, only results obtained with stronger pairing are shown. According to our calculations (see also Ref. [4]), pairing correlations do not influence the values of S_{2n} very much: the only noticeable differences occur for the very last stable isotopes (cf. results for Ar in Fig. 2). On the other hand, the differences between the

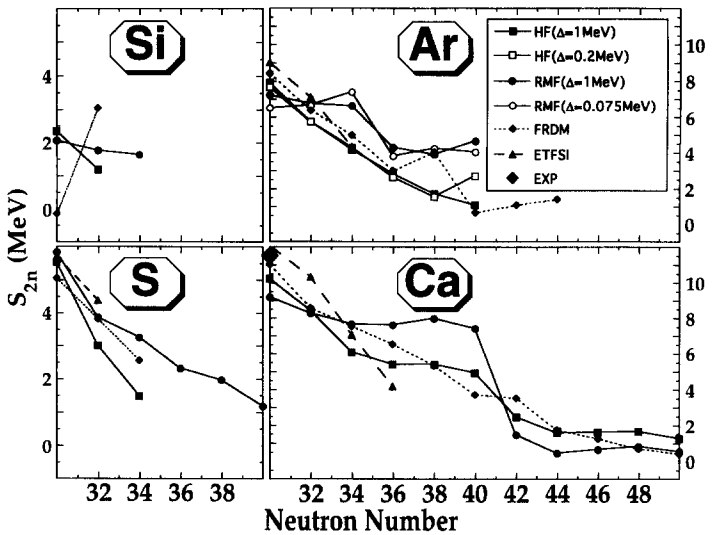

Fig. 2. Same as Fig. 1, except for the heaviest isotopes. HF (filled squares) and RMF (filled circles) results were obtained with stronger pairing. To illustrate the effect of the pairing strength on S_{2n}, the results of weaker-pairing calculations are shown for Ar isotopes (open symbols).

models are quite significant for the whole region of neutron-rich nuclei. Generally, the RMF calculations predict more binding than the HF, except for the Ca isotopes, where a strong shell effect at $N = 40$ causes S_{2n} to drop rapidly in the RMF model.

For the Si isotopes, the heaviest bound nucleus predicted in the HF+SIII model is $^{46}Si_{32}$. In this nucleus, the last occupied neutron orbital is $2p_{3/2}$, while $2p_{1/2}$ has already positive energy. In the RMF model, the $2p_{1/2}$ orbital is still bound, and $^{48}Si_{34}$ is calculated to be the last bound isotope. Values of S_{2n} predicted by the FRDM for the Si isotopes show very irregular behavior. However, the very location of the neutron drip line agrees with the HF results.

For the S isotopes, the difference in the location of the two-neutron drip line between HF and RMF models is more significant. The HF model (in both SIII and SkM* parametrizations) predicts $^{50}S_{34}$ as the last two-neutron stable nucleus. In the HF model this isotope is deformed with $\beta_2 \approx 0.15$ in SIII parametrization and $\beta_2 \approx 0.10$ with SkM* parameters (cf. Section 3.2). The RMF model, again, predicts stronger binding and larger shell gaps: in contrast to the HF model, all the pf-shell orbitals are calculated to be bound. Consequently, in this model, three additional even–even S isotopes are predicted to be two-neutron stable, the last being spherical $^{56}S_{40}$. FRDM predictions agree with HF results.

Both HF and RMF models calculate the last two-neutron stable isotope of Ar at $N = 40$. The two-neutron separation energy of this isotope is still relatively large, particularly in the RMF model (~ 4 MeV). This can be understood as an effect of $N = 40$ subshell closure below the $1g_{9/2}$ orbital. The FRDM S_{2n} values are again irregular.

A stabilizing effect of the proton shell closure at $Z = 20$ manifests itself by a

substantial increase in the number of stable isotopes when going from Ar to Ca. The RMF, HF+SIII and FRDM models predict the two-neutron stability of all isotopes through $N = 50$, i.e. to the next neutron shell closure. (In the HF+SkM* model, four more even–even Ca isotopes are expected to be bound.) As one can see in Fig. 2, the two-neutron separation energy for the Ca isotopes with neutron number in excess of 40 is almost constant in all models.

It is interesting to compare the predictions of HF, RMF and FRDM with those obtained within HFB theory, in which pairing correlations are treated more consistently [5,37]. The calculations in Refs. [5,37] were performed for spherical shapes only, but in the present calculations the very last bound isotopes (except for sulfur in the HF model) are predicted to be spherical. The spherical HFB model with the SkP parametrization predicts that the last two-neutron stable isotopes of Si, S, Ar and Ca correspond to $N = 34$, 36, 42 and 48, respectively. This indicates that shell-closure effects at neutron numbers 40 and 50 are more pronounced in the models discussed in this study than they are in the HFB+SkP model. (This can be attributed to different effective mass, see Ref. [38].) The question of the shell structure in nuclei close to the drip lines is of particular importance in astrophysical applications and requires a detailed theoretical analysis (as well as new tools and methods to carry it out).

3.2. Deformations

The ground-state minima of Si, S and Ar isotopes studied in this work correspond, in most cases, to deformed intrinsic states. The Ca isotopes are calculated to be spherical. The minima obtained in HF calculations turned out to correspond to reflection-symmetric shapes with three symmetry planes, i.e. $\langle x\rangle = \langle y\rangle = \langle z\rangle = 0$ and $\langle xy\rangle = \langle xz\rangle = \langle yz\rangle = 0$. Consequently, the moments $q_{\lambda\mu}$ with odd λ or μ vanish. In order to compare various variants of calculations and to relate them to previous works, the quadrupole deformation parameters β_2 and γ were extracted. Firstly, the two quadrupole moments, q_{20} and q_{22}, were expressed in terms of the polar coordinates Q_0 and γ

$$q_{20} = Q_0 \cos\gamma, \qquad q_{22} = \frac{1}{\sqrt{2}} Q_0 \sin\gamma. \tag{2}$$

The proton quadrupole moment, Q_0^{p}, can be written in terms of the proton quadrupole deformation, β_2^{p}, by means of the relation

$$Q_0^{\mathrm{p}} = \sqrt{\frac{5}{\pi}} Z \langle r_{\mathrm{p}}^2\rangle \beta_2^{\mathrm{p}}. \tag{3}$$

Similarly, one can extract quadrupole deformations of the neutron (β_2^{n}) and mass (β_2^{A}) distribution. (For axial shapes, we adopted the standard convention, i.e. $\beta_2 > 0$ (prolate) for $\gamma \sim 0°$ and $\beta_2 < 0$ (oblate) for $\gamma \sim 60°$.)

The predicted mass quadrupole deformations as a function of N are shown in Fig. 3 (Si), Fig. 4 (S) and Fig. 5 (Ar). In the figures, the position of the second minima is also indicated together with their energy relative to the lowest minimum.

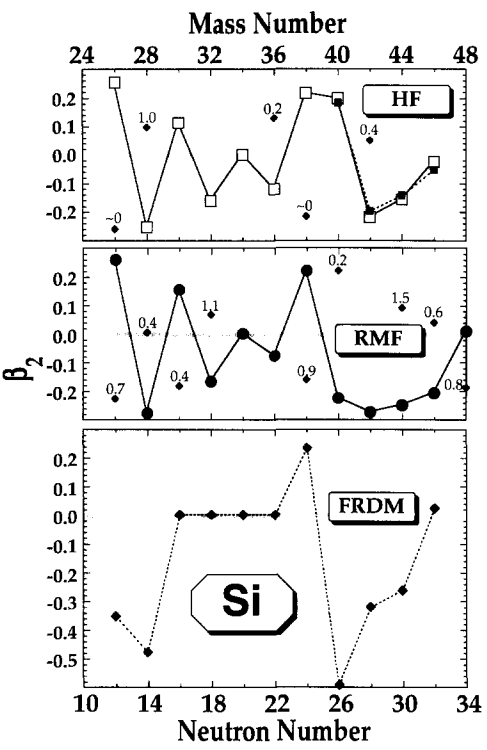

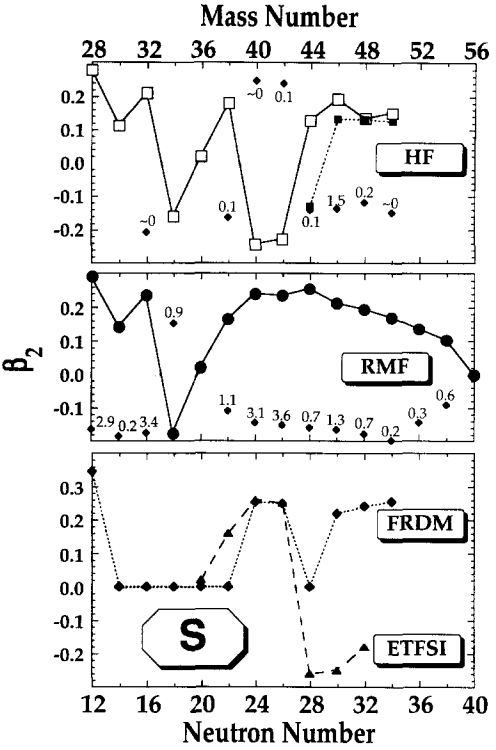

Fig. 3. Equilibrium deformation β_2 of Si isotopes calculated in HF (top part), RMF (middle) and FRDM (bottom) models. Filled squares in the upper part correspond to stronger pairing. In RMF calculations, the results with stronger and weaker pairing are very similar. Diamonds indicate the deformation of the second minimum, with its excitation energy given in MeV.

Fig. 4. Same as Fig. 3, except for S isotopes. In the bottom part of the figure, the results of ETFSI calculations are also indicated.

The results for the Si isotopes are similar in both RMF and HF models. The $N = 12$ isotope is predicted to be prolate with $\beta_2 \approx 0.25$. However, the secondary, oblate minimum is predicted to lie very close in energy. As expected, the $N = Z$ isotope, $^{28}Si_{14}$, is oblate in all models, including FRDM. (The same result was obtained in the framework of HF+SkI and HF+SkII models [13], and in relativistic models of Refs. [17,18].) This can be understood from the corresponding level scheme (Fig. 3 in Ref. [9]): one can see that the $N = 14$ gap between $1d_{5/2}$ and $2s_{1/2}$ orbitals slightly favors oblate shapes, while the $N = 16$ gap between $2s_{1/2}$ and $1d_{3/2}$ increases with increasing deformation, thus favoring prolate shapes. Indeed, the $N = 16$ isotope has $\beta_2 \approx 0.15$ in both RMF and HF models. (It is, however, spherical in FRDM calculations.) The same level scheme indicates that the $N = 18$ gap is more pronounced on the oblate side and, consistently with this picture, $^{32}Si_{18}$ has oblate deformation in both RMF and HF models (FRDM predicts the spherical shape). Let us notice here that *all* isotones with $N = 18$, i.e. ^{32}Si, ^{34}S and ^{36}Ar, are oblate in HF and RMF calculations. Shell closure at $N = 20$ stabilizes the spherical shape of ^{34}Si in all models considered.

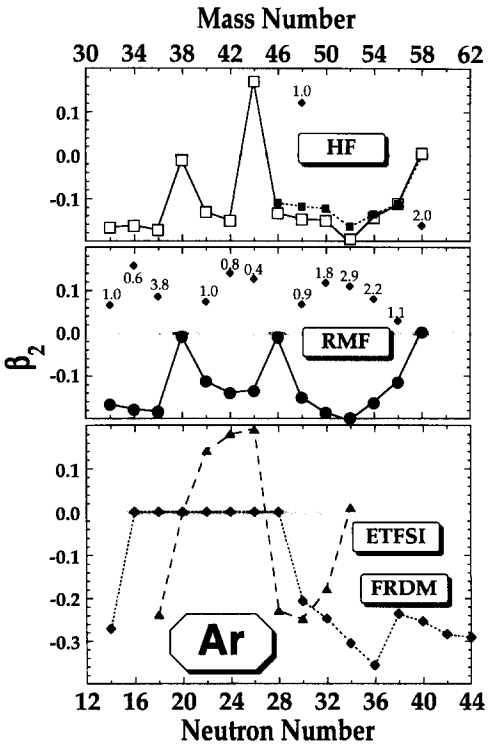

Fig. 5. Same as Fig. 4, except for Ar isotopes.

It is interesting to note that the $N = 28$ shell closure does not support the spherical shape in the ^{42}Si isotope: all models predict oblate deformation. (The excited prolate configuration lies only slightly higher in energy.) The Si isotopes with $N > 28$ also have oblate deformations in all the models considered, with β_2 approaching zero for the neutron drip-line nuclei (^{46}Si in HF and FRDM, and ^{48}Si in RMF calculations). As can be seen in Fig. 3, the prolate–oblate energy difference is usually not very large (especially in the HF model): this indicates that the Si isotopes are generally γ-soft and their deformation is sensitive to fine details of the single-particle spectrum.

Equilibrium deformations of the S isotopes (Fig. 4) were discussed in Ref. [9]. The proton number $Z = 16$ favors prolate deformations (see Fig. 3 in Ref. [9]), and this is indeed visible when one compares deformations of Si and S isotones. The nucleus $^{32}S_{16}$ is predicted to be prolate (in agreement with HFB+Gogny [15], HF+SkI and HF+SkII [13], and RMF [17,18] calculations). For the $N = 28$ isotope, equilibrium deformation corresponds to prolate shape, but the oblate configuration is almost degenerate. (Actually, as can be seen in the figure, the oblate minimum becomes lower in energy when stronger pairing is used in the HF model.) The HF+SkM* model predicts smaller ($\beta_2 \approx 0.1$) deformation of ^{44}S. In both RMF and HF models, isotopes with $N > 28$ have prolate deformation, the secondary oblate minimum being very close in energy. One can thus conclude that the S isotopes are generally γ-soft, with prolate

and oblate configurations almost degenerate. (This applies especially to the results of the HF+SIII model.) The FRDM model predicts prolate shapes for the heavier S isotopes, with the exception of ^{44}S, which is calculated to be spherical. The results of ETFSI calculations for the heavy S isotopes ($A \geqslant 34$) are in disagreement with all the three models discussed: they are predicted to have oblate shape. Both FRDM and ETFSI models calculate spherical shapes for $^{30-36}S_{14-20}$. It is interesting to note that HF+SkM* also yields a spherical shape for these isotopes, indicating $N = 14$ sub-shell closure. RMF and HF+SIII models predict prolate deformation for $^{30-32}$S and oblate for ^{34}S. This is consistent with experimental estimates of deformation (based on $B(E2)$ measurements) which suggest large deformation of $^{30-34}$S and small (or vanishing) for ^{36}S [39].

As has already been mentioned, particle number 18 tends to favor oblate shapes. The calculated deformations of Ar isotopes (Fig. 5) are consistent with this picture, as are the results of previous calculations for $^{36}Ar_{18}$ [13,17,18]. In the RMF model, they all correspond to oblate shapes, except for $^{38}Ar_{20}$, $^{46}Ar_{28}$ and $^{58}Ar_{40}$, which are spherical. In the HF model $^{38}Ar_{20}$ and $^{58}Ar_{40}$ are spherical; all other isotopes have oblate ground states, except for $^{44}Ar_{26}$ which, according to HF calculations, is triaxial. The $N = 28$ isotope, ^{46}Ar, is predicted to be deformed, indicating that the shell effect at $N = 28$ is weak in the HF+SIII model. In FRDM calculations, the Ar isotopes are either spherical ($N \leqslant 28$) or oblate. The effect of subshell closure at $N = 40$ is not visible: the nucleus $^{58}Ar_{40}$ is a well-deformed oblate system. In contrast to other calculations, the ETFSI model predicts prolate deformations for isotopes with $N = 22$, 24 and 26 ($^{46}Ar_{28}$ is predicted to be oblate).

Generally, Si, S and Ar isotopes can be considered as γ-soft, with deformations depending on subtle interplay between the deformed gaps $Z = 16$ and 18, $N = 28$, and the spherical gap at $N = 28$. In particular, cross-shell excitations to the $2p_{3/2}$, $2p_{1/2}$and $1f_{5/2}$ shells cannot be neglected: the $N = 28$ gap appears to be broken in most cases [9].

The differences between neutron and proton deformations, $\Delta|\beta_2| \equiv |\beta_2^n| - |\beta_2^p|$, are shown in Fig. 6. Both HF and RMF models predict the proton deformation to be smaller for very proton-rich isotopes of Si, S and Ar. As the neutron number increases, approaching the neutron drip line, $|\beta_2^n|$ becomes smaller than $|\beta_2^p|$ by a few hundredths. The effect is particularly pronounced in the RMF model for the neutron-rich silicon and sulfur isotopes. The largest difference is obtained for $^{54}S_{38}$, where $\Delta|\beta_2|$ reaches -0.10. Systematically, when the excess of neutrons (or protons) becomes large, $\Delta|\beta_2|$ increases in magnitude. (The effect is much weaker in the HF+SkM* model, where $\Delta|\beta_2|$ is noticeably different from zero only for the Ar isotopes, cf. Fig. 6.) This phenomenon, if confirmed experimentally, might give rise to isovector quadrupole modes with interesting rotational behavior and unusual magnetic properties. One has to bear in mind, however, that the standard BCS-like treatment of pairing (as employed in this study) has certain drawbacks when applied to extremely neutron- or proton-rich isotopes. When the Fermi energy approaches zero, the BCS model leads to non-localized wave functions [6]. To avoid this problem, one can use a model with no or very weak pairing, as was done in one variant of calculations presented in this study. It

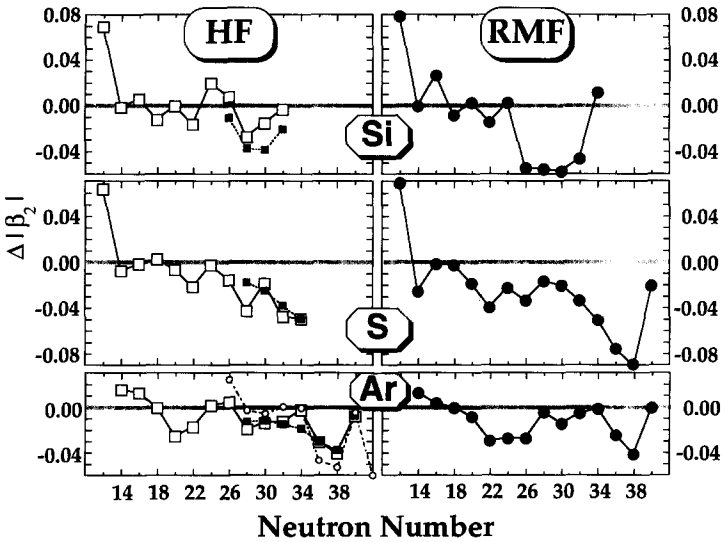

Fig. 6. Difference $\Delta|\beta_2| \equiv |\beta_2^n| - |\beta_2^p|$ for the even–even Si, S and Ar isotopes calculated in HF (left) and RMF (right) models as a function of neutron number. Filled squares in the left panel correspond to stronger pairing. Open circles for Ar isotopes (in the part corresponding to HF calculations) indicate the results obtained in HF+SkM*.

is known, however, that pairing correlations *do* play an important role in the drip-line systems, as several measurable quantities (like nuclear radii) are very sensitive to pairing correlations [4,5,37]. This problem may be overcome in the HFB method with a realistic pairing interaction in which the coupling of bound states to a particle continuum is correctly taken into account [4]. Preliminary results, obtained with the *spherical* HFB+SkP model, indicate that drip-line nuclei indeed exhibit a host of new and sometimes unexpected properties [5,7,37,38,40].

3.3. Radii

The predicted root-mean-square (rms) radii of even–even Si, S, Ar and Ca isotopes are illustrated in Fig. 7 (charge radii) and Fig. 8 (neutron radii). Experimental data on the charge radii of Si, S, Ar and Ca isotopes are also summarized in Table 1. Both models yield charge radii close to experimental data, although RMF (and HF+SkM*) values are systematically smaller (by ~0.08 fm) than those obtained with the HF+SIII model. In Fig. 7, the values obtained in the ETFSI model are also indicated for comparison. One can see that the ETFSI model agrees better with the RMF predictions for smaller neutron numbers, and with the HF predictions for larger values of N. None of the three models is able to reproduce the experimentally observed decrease of the charge radius of Ca isotopes with $24 \leqslant N \leqslant 28$. In the RMF calculation, however, at least a plateau, absent in the two other models, is clearly visible. An increase of charge radii with decreasing neutron number is predicted for the lightest isotopes of Si and S. This may be understood as a manifestation of the proton skin. The neutron radii (Fig. 8)

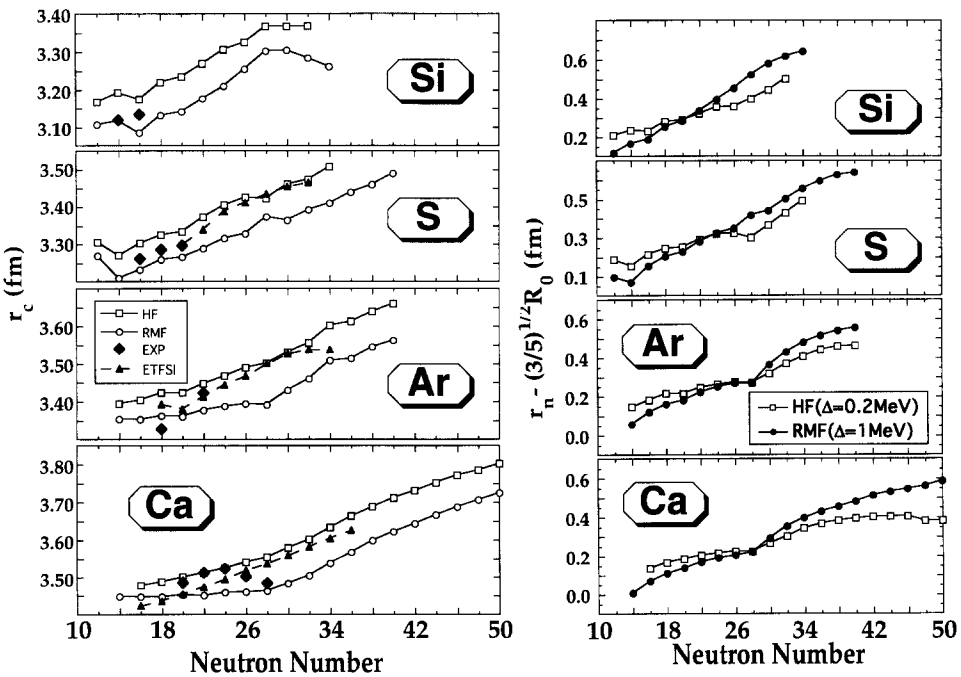

Fig. 7. Root-mean-square radii of the charge distribution of the even–even Si, S, Ar and Ca isotopes calculated with the RMF (circles), HF (squares), and ETFSI (triangles) models. Experimental values are marked by filled diamonds connected with a dashed line (see also Table 1).

Fig. 8. Root-mean-square neutron radii of the even–even Si, S, Ar and Ca isotopes calculated with the RMF (circles) and HF (squares) models. The radii are shown relative to the average value of $\sqrt{3/5}R_0$, $R_0 = 1.2A^{1/3}$ fm.

Table 1
Experimental and predicted rms charge radii $\langle r_c^2 \rangle^{1/2}$ (in fm) of Si, S, Ar and Ca isotopes. The experimental data are taken from Refs. [41] (Si), [42] (S), [43] (Ar) and [44] (Ca)

Nucleus	Exp	HF	RMF	ETFSI
^{28}Si	3.120(7)	3.19	3.13	
^{30}Si	3.134(7)	3.17	3.10	
^{32}S	3.261(1)	3.30	3.25	
^{34}S	3.284(2)	3.32	3.27	
^{36}S	3.297(1)	3.33	3.27	3.30
^{36}Ar	3.327(15)	3.42	3.37	3.39
^{40}Ar	3.423(14)	3.44	3.38	3.41
^{40}Ca	3.4852(33)	3.50	3.46	3.45
^{42}Ca	3.5125(50)	3.51	3.46	3.47
^{44}Ca	3.5231(50)	3.52	3.46	3.50
^{46}Ca	3.5022(50)	3.54	3.46	3.52
^{48}Ca	3.4837(46)	3.55	3.47	3.54

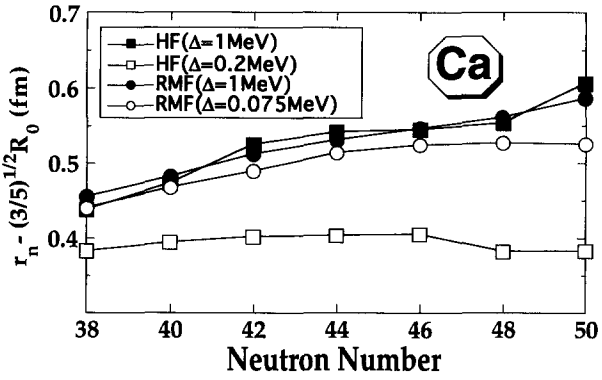

Fig. 9. Root-mean-square neutron radii of $^{58-70}$Ca isotopes calculated with HF+SIII (squares) and RMF (circles) models with stronger (filled symbols) and weaker (open symbols) pairing. The radii are shown relative to the average value of $\sqrt{3/5}R_0$, $R_0 = 1.2A^{1/3}$ fm.

increase monotonically with increasing neutron number, and for neutron-rich nuclei are much larger that those of the proton distribution (neutron skin). A shell-closure effect is visible for Ar and Ca isotopes with $N = 28$, and for ^{44}S in the HF model. In RMF calculations the same nucleus exhibits an *increase* of neutron radius, confirming that the $N = 28$ gap is completely broken in this model.

For nuclei close to the stability line, the pairing strength does not influence the results for the radii very much, at least in the considered configuration space. However, when approaching the drip lines, the results depend strongly on pairing, especially in the HF calculations. This is illustrated in Fig. 9 which shows a neutron radius (relative to liquid-drop estimate) for weakly bound $^{58-70}$Ca isotopes calculated with two different values of pairing-gap parameter Δ (= 200 keV and 1 MeV for HF calculations, and 75 keV and 1 MeV for the RMF model). One can see that at the drip line, neutron radii calculated in the HF model with stronger pairing are larger than those corresponding to weaker pairing by ~ 0.20 fm (the difference is smaller in RMF calculations). This can be understood as the manifestation of the neutron gas effect in the BCS model: as the Fermi energy approaches zero, unbound positive energy levels contribute to the total wave function leading to a spatially extended nucleonic density. Although the effect of a neutron halo is physically possible, its description in terms of standard BCS theory involves unbound orbitals and is therefore unreliable. In the RMF model the influence of pairing on neutron radii is much less pronounced. This can be attributed to the fact that in this model the calculations were performed in the harmonic-oscillator basis. The use of the harmonic-oscillator basis artificially confines the wave function: the neutron gas effect is much weaker, but the description of very weakly bound states is also unreliable, due to the wrong asymptotic behavior of wave functions [38]. A consistent description of nuclear radii, which includes pairing correlations and correct asymptotic behavior of wave functions, can be achieved within the HFB model [37].

4. Conclusions

The calculations presented in this article confirm strong deformation effects for $N \approx 28$ isotones due to $1f_{7/2} \rightarrow fp$ core breaking, especially in the RMF model. Deformation dependence of a single-particle spectrum favors prolate shapes for $N = 16$ and oblate for $N = 18$. Generally, almost all deformed nuclei in the region considered here are γ-soft. The results also suggest a possibility of large isovector-deformation effects for exotic nuclei, in particular those close to the neutron drip line. The results obtained with the two models considered, HF and RMF, are similar, although the RMF (and the HF+SkM*) model predicts systematically more binding. It has also been shown that a detailed analysis of drip-line nuclei, in particular their radii, requires a new approach which would allow for a correct description of interplay between pairing correlations and mean-field properties, and of the asymptotic behavior of wave functions of very weakly bound systems.

Acknowledgements

Oak Ridge National Laboratory is managed for the US Department of Energy by Lockheed Martin Energy Systems under Contract No. DE-AC05–84OR21400. The Joint Institute for Heavy Ion Research has as member institutions the University of Tennessee, Vanderbilt University and the Oak Ridge National Laboratory; it is supported by the members and by the Department of Energy through Contract No. DE-FG05-87ER40361 with the University of Tennessee. Theoretical nuclear physics research is supported by the US Department of Energy through Contracts No. DE-FG05-93ER40770 (University of Tennessee), DE-FG05-87ER40376 (Vanderbilt University) and DE-FG02-94ER40834 (University of Maryland). The numerical calculations were partially carried out on supercomputers at the National Energy Research Supercomputing Center, Livermore. This work was partially supported by the Polish Committee for Scientific Research under Contract No. 2 P03B 034 08.

References

[1] Physics and Techniques of Secondary Nuclear Beams, eds. J.F. Bruandet, B. Fernandez and M. Bex (Editions Frontières, Gif-sur-Yvette, 1992).
[2] E. Roeckl, Rep. Prog. Phys. 55 (1992) 1661.
[3] A. Mueller and B. Sherril, Ann. Rev. Nucl. Part. Sci. 43 (1993) 529.
[4] J. Dobaczewski, H. Flocard and J. Treiner, Nucl. Phys. A 422 (1984) 103.
[5] J. Dobaczewski, W. Nazarewicz and T.R. Werner, Phys. Scr. 56 (1995) 15.
[6] W. Nazarewicz, T.R. Werner and J. Dobaczewski, Phys. Rev. C 50 (1994) 2860.
[7] W. Nazarewicz, J. Dobaczewski and T.R. Werner, Phys. Scr. 56 (1995) 9.
[8] W. Nazarewicz, J. Dobaczewski, T.R. Werner, J.A. Maruhn, P.-G. Reinhard, K. Rutz, C.R. Chinn, A.S. Umar and M.R. Strayer, to be published.
[9] T.R. Werner, J.A. Sheikh, W. Nazarewicz, M.R. Strayer, A.S. Umar and M. Misu, Phys. Lett. B 333 (1994) 303.

[10] O. Sorlin, D. Guillemaud-Mueller, A.C. Mueller, V. Borrel, S. Dogny, F. Pougheon, K.-L. Kratz, H. Gabelmann, B. Pfeiffer, A. Wohr, W. Ziegert, Yu.E. Penionzhkevich, S.M. Lukyanov, V.S. Salamatin, R. Anne, C. Borcea, L.K. Fifield, M. Lewitowicz, M.G. Saint-Laurent, D. Bazin, C. Detraz, F.-K. Thielemann and W. Hillebrandt, Phys. Rev. C 47 (1993) 2941.
[11] R. Schneider et al., Z. Phys. A 348 (1994) 241.
[12] G.A. Leander and S.E. Larsson, Nucl. Phys. A 239 (1975) 93.
[13] H.R. Jaqaman and L. Zamick, Phys. Rev. C 30 (1984) 1719.
[14] H. Flocard, P.H. Heenen, S.J. Krieger and M. Weiss, Prog. Theor. Phys. 72 (1984) 1000.
[15] M. Girod and B. Grammaticos, Phys. Rev. C 27 (1983) 2317.
[16] R.J. Furnstahl, C.E. Price and G.E. Walker, Phys. Rev. C 36 (1987) 2590.
[17] J. Fink, V. Blum, P.-G. Reinhard, J. Maruhn and W. Greiner, Phys. Lett. B 218 (1989) 277.
[18] S.K. Patra and C.R. Praharaj, Nucl. Phys. A 565 (1993) 442.
[19] J.-K. Zhang and D.S. Onley, Phys. Rev. C 49 (1994) 762.
[20] M. Carchidi, B.H. Wildenthal and B.A. Brown, Phys. Rev. C 34 (1986) 2280.
[21] J. Zhang, W.D.M. Rae and A.C. Merchant, Nucl. Phys. A 575 (1994) 61.
[22] J.L. Wood, K. Heyde, W. Nazarewicz, M. Huyse and P. van Duppen, Phys. Reports 215 (1992) 101.
[23] X. Campi, H. Flocard, A.K. Kerman and S. Koonin, Nucl. Phys. A 251 (1975) 193.
[24] R. Bengtsson, P. Möller, J.R. Nix, J.-y. Zhang, Phys. Scr. 29 (1984) 402.
[25] A. Poves and J. Retamoso, Phys. Lett. B 184 (1987) 311.
[26] E.K. Warburton, J.A. Becker and B.A. Brown, Phys. Rev. C 41 (1990) 1147.
[27] K. Heyde and J.L. Wood, J. Phys. G 17 (1991) 135.
[28] E. Caurier, A.P. Zuker, A. Poves and G. Martínez-Pinedo, Phys. Rev. C 50 (1994) 225.
[29] A.S. Umar, J.-S. Wu, M.R. Strayer and C. Bottcher, J. Comp. Phys. 93 (1991) 426.
[30] A.S. Umar, M.R. Strayer, J.-S. Wu, D.J. Dean and M.C. Güçlü, Phys. Rev. C 44 (1991) 2512.
[31] M. Beiner, H. Flocard, N. Van Giai and P. Quentin, Nucl. Phys. A 238 (1975) 29.
[32] J. Bartel, P. Quentin, M. Brack, C. Guet and H.B. Håkansson, Nucl. Phys. A 386 (1982) 79.
[33] B.D. Serot and J.D. Walecka, Adv. Nucl. Phys. 16 (1986) 1.
[34] M.M. Sharma, M.A. Nagarajan and P. Ring, Phys. Lett. B 312 (1993) 377.
[35] P. Möller, J.R. Nix, W.D. Myers and W.J. Swiatecki, At. Data Nucl. Data Tables 59 (1995) 185.
[36] Y. Aboussir, J.M. Pearson, A.K. Dutta and F. Tondeur, Nucl. Phys. A 549 (1992) 155; J.M. Pearson, private communication (1993).
[37] J. Dobaczewski, W. Nazarewicz and T.R. Werner, Z. Phys., 1995, in press.
[38] J. Dobaczewski, W. Nazarewicz, T.R. Werner, J.-F. Berger, C.R. Chinn and J. Dechargé, to be submitted to Phys. Rev. C.
[39] S. Raman, C.H. Malarkey, W.T. Milner, C.W. Nestor Jr. and P.H. Stelson, At. Data Nucl. Data Tables 36 (1987) 1.
[40] B. Chen, J. Dobaczewski, K.-L. Kratz, K. Langanke, B. Pfeiffer, F.-K. Thielmann and P. Vogel, Phys. Lett. B 355 (1995) 37.
[41] G. Fricke, J. Heberz, Th. Hennemann, G. Mallot, L.A. Schaller, L. Schellenberg, C. Piller and R. Jacot-Guillarmod, Phys. Rev. C 45 (1992) 80.
[42] L.A. Schaller, D.A. Barandao, P. Bergem, M. Boschung, T.Q. Phan, G. Piller, A. Rüetschi, L. Schellenberg, H. Schneuwly, G. Fricke, G. Mallot and H.G. Sieberling, Phys. Rev. C 31 (1985) 1007.
[43] H. de Vries, C.W. De Jager and C. de Vries, At. Data Nucl. Data Tables 36 (1987) 495.
[44] E.G. Nadjakov, K.P. Marinova and Yu.P. Gangrsky, At. Data Nucl. Data Tables 56 (1994) 133.